J. Fluid Mech. (2010), *vol.* 651, *pp.* 519–539. © Cambridge University Press 2010
doi:10.1017/S002211200999423X

Channel flow over large cube roughness: a direct numerical simulation study

STEFANO LEONARDI[1] AND IAN P. CASTRO[2]†

[1]Department of Mechanical Engineering, University of Puerto Rico, Mayaguez 00680, Puerto Rico
[2]School of Engineering Sciences, University of Southampton, Southampton SO17 1BJ, UK

(Received 17 September 2009; revised 22 December 2009; accepted 22 December 2009;
first published online 7 April 2010)

Computations of channel flow with rough walls comprising staggered arrays of cubes having various plan area densities are presented and discussed. The cube height h is 12.5 % of the channel half-depth and Reynolds numbers ($u_\tau h/\nu$) are typically around 700 – well into the fully rough regime. A direct numerical simulation technique, using an immersed boundary method for the obstacles, was employed with typically 35 million cells. It is shown that the surface drag is predominantly form drag, which is greatest at an area coverage around 15 %. The height variation of the axial pressure force across the obstacles weakens significantly as the area coverage decreases, but is always largest near the top of the obstacles. Mean flow velocity and pressure data allow precise determination of the zero-plane displacement (defined as the height at which the axial surface drag force acts) and this leads to noticeably better fits to the log-law region than can be obtained by using the zero-plane displacement merely as a fitting parameter. There are consequent implications for the value of von Kármán's constant. As the effective roughness of the surface increases, it is also shown that there are significant changes to the structure of the turbulence field around the bottom boundary of the inertial sublayer. In distinct contrast to two-dimensional roughness (longitudinal or transverse bars), increasing the area density of this three-dimensional roughness leads to a monotonic decrease in normalized vertical stress around the top of the roughness elements. Normalized turbulence stresses in the outer part of the flows are nonetheless very similar to those in smooth-wall flows.

1. Introduction

Despite increased attention over recent years, the nature of the atmospheric flow over heterogeneous collections of buildings and other man-made structures remains incompletely understood. Even for neutral atmospheres a number of basic questions are still unresolved. For example, although data from a number of field studies over medium-to-large cities have been analysed in order to determine the relationships between surface morphology and total surface drag there is still uncertainty regarding such relationships. In their comprehensive survey of available field data, Grimmond & Oke (1999) stated that 'the lack of a sizable and authoritative body of measured values means that there is no credible standard against which to validate morphometric formulae', a claim based on their conclusion that 'there are few credible estimates of

† Email address for correspondence: i.castro@soton.ac.uk

https://doi.org/10.1017/S002211200999423X Published online by Cambridge University Press

urban y_o'. (y_o is the surface roughness parameter defined through the usual log-law mean flow profile). Field studies undertaken since then would not lead to markedly different conclusions. One of the simplest questions (at least to ask) concerns the plan area density of the building array which yields maximum surface drag. The answer must naturally depend on the specific building shapes and orientations, but even for the arguably simplest case of uniformly staggered arrays of cubes there remains some uncertainty. Santiago *et al.* (2008) recently addressed this problem computationally, using classical Reynolds-averaged Navier–Stokes (RANS) computations. Their results were, overall, not dissimilar to those deduced on the basis of the rather limited laboratory measurements available. However, as they admitted, the results suffer from the inevitable uncertainties arising from using RANS for what is a highly complex three-dimensional flow with regions of strong local pressure gradients, mean flow strains, reversed flow and high-turbulence intensities (see § 4).

With the increasing levels of computer power now available, a number of authors have employed direct numerical simulation (DNS) and large eddy simulation (LES) to explore flows over arrays of sharp-edged elements – Stoesser *et al.* (2003), Kanda, Moriwaki & Kasamatsu (2004), Coceal *et al.* (2006, 2007*b*), Coceal, Thomas & Belcher (2007*a*), Xie & Castro (2006), Xie, Coceal & Castro (2008) and Orlandi & Leonardi (2006) provide the majority of such studies, but see also Bhaganagar, Kim & Coleman (2004) for DNS over roughness characterized by elements *not* having sharp edges. These have all been of single (or sometimes two) specific roughness arrays but they have shown unequivocally that such approaches are far superior to RANS methods and can be used successfully to explore the detailed nature of the flow within and above the canopy region. (The study by Coceal *et al.* 2006 for a staggered cube array provided the benchmark DNS that Santiago *et al.* 2008 used to assess the accuracy of their RANS computations.) In this paper we report results of a set of DNS computations for staggered cube arrays having λ_p, the plan area coverage density, varying from 0.04 to 0.25. Unlike the method used by Coceal *et al.* (2006), the code employed here is of the immersed boundary variety; this allows non-uniform grids to be used more easily so that mesh resolution within the canopy, especially close to all solid surfaces, is significantly higher than anything used previously for these kind of flows. Since it was anticipated that the frictional drag contribution to the total drag might be non-negligible at the lower values of λ_p (unlike at higher values where the form drag dominates overwhelmingly), such resolution was thought likely to be particularly important.

Attention is concentrated in this paper on the mean flow field. We discuss both how the surface drag components vary with λ_p and the implications of the data for the mean velocity log law. The usual definition of a fully rough-wall condition is that frictional contributions to the wall drag are negligible – all the wall drag arises from pressure forces acting on the roughness elements. This, incidentally, means that the viscous length scale (ν/u_τ) is not a relevant near-wall scale and such flows are therefore much less dependent on Reynolds numbers, like the momentum thickness Reynolds number Re_θ, than are smooth-wall flows (Castro 2007). An immediate consequence is that the high Reynolds numbers usually thought necessary before one can expect a substantial log law might, for fully rough-wall flows, be rather lower. In any case, rough-wall flows of the type considered here require careful consideration of the effective origin of the wall-normal coordinate. It was perhaps Perry, Schofield & Joubert (1969) who first emphasized the complications posed by roughness because of the shift in the effective $y = 0$ location. For most of their roughnesses, as for all cases when the roughness height is very small compared with the boundary layer

https://doi.org/10.1017/S002211200999423X Published online by Cambridge University Press

depth, there was no chance of making measurements within the roughness array itself, whereas for the larger roughness (comprising sharp-edged rectangular blocks) as in the present case, it was possible to determine the pressure drag forces by obtaining pressure fields around the obstacles.

There has been considerable discussion, particularly over the last decade or so, concerning the value of von Kármán's coefficient κ both in smooth-wall (engineering type) flows and the atmospheric boundary layer, where the surface is almost invariably fully rough. There is controversy in both camps. For the former, Nagib & Chauhan (2008) review some of the recent data and conclude that κ is not universal but rather is flow dependent. In the atmospheric surface layer, there is evidence that κ falls with increasing roughness Reynolds number ($u_\tau y_o/\nu$). Frenzen & Vogel (1995), for example, in reviewing the half-century history of evaluation of κ from such measurements conclude that it varies 'from a maximum of 0.41 in light winds over open water and smooth land surfaces to a minimum of 0.37 in stronger winds over forests and cities'. (This range brackets the continuous range of values suggested by Nagib & Chauhan (2008) for smooth-wall flows of different types.) Likewise, Oncley *et al.* (1996) found that κ falls slowly with increasing roughness Reynolds number. However, field measurements are bedeviled by relatively large scatter, the possible influences of thermal stability and, for large roughness elements, uncertain but definitely non-zero offsets in the effective surface height (usually termed the 'zero-plane displacement'). Some authors therefore go no further than stating that there is no compelling evidence that κ is independent of roughness Reynolds number (Andreas & Trevino 2000). More recently, Andreas *et al.* (2006) have argued that the apparent fall in κ with $u_\tau y_o/\nu$ cannot be distinguished statistically from an 'artificial fall' inherent in the log-law relationship. In any case, there does seem to be a consensus that in the atmospheric boundary layer (almost always fully rough) κ is measurably lower than the classical smooth-wall value around 0.4; as a very recent example, Li, Zimmerman & Princevac (2008) find a value of 0.36 for neutral flow over a site in Washington State (USA), where the surface 'was covered by sparse sagebrush and grass, with no fully vegetated canopy present'. In that case, there can be little doubt about the essentially zero value for the zero-plane displacement d. Another example of a wall flow apparently yielding lower values of κ is the DNS study of Breugrem, Boersma & Uittenbogaard (2006), who considered wall permeability in channel flow. Because of the porous wall condition they too had to consider shifts in the vertical origin and they obtained values of κ down to as low as 0.31. In the present paper, we suggest that because DNS of very rough surface flows (in a channel) allows precise determination of a physically based zero-plane displacement as well as the total wall drag, conclusions about the log law are less susceptible to 'measurement' uncertainties. The present data certainly have implications for the log law and von Kármán's coefficient, as we demonstrate.

Some features of the basic turbulence fields are also explored briefly in this paper, not least because they allow one to assess the adequacy of the hypothesis (usually attributed to Townsend) that surface roughness merely changes the wall stress but not the structure of the boundary layer. There is contradictory evidence in the literature, particularly in the context of boundary layers (e.g. Krogstad & Antonia 1999). Some comments about the turbulence within the canopy region (i.e. below the top of the roughness) are also made, with reference to the dispersive stresses which arise because of the strong inhomogeneities in the flow there. A more comprehensive study of the nature of the turbulence both within and above the canopy will be presented in a subsequent paper.

https://doi.org/10.1017/S002211200999423X Published online by Cambridge University Press

The numerical method is outlined in the following section, § 3 presents results for global quantities like the drag components, y_o, d and the log law, and some brief discussion of the turbulence characteristics is given in § 4. Conclusions are summarized in § 5.

2. Numerical procedures

The non-dimensional Navier–Stokes and continuity equations for incompressible, neutrally stable flows can be expressed as

$$\frac{\partial U_i}{\partial t} + \frac{\partial U_i U_j}{\partial x_j} = -\frac{\partial P}{\partial x_i} + \frac{1}{Re}\frac{\partial^2 U_i}{\partial x_j^2} + \Pi\delta_{i1}, \quad \nabla \cdot \boldsymbol{U} = 0, \tag{2.1}$$

where Re is the Reynolds number based on the cube height h and the bulk velocity ($U_b = 1/H \int_0^H U \mathrm{d}y$), which is held constant in time, δ_{ij} is the Kronecker delta, U_i is the component of the velocity vector in the i direction and P is the pressure per unit mass. The quantity Π is the pressure gradient required to maintain the constant flow rate and thus varies with time. This method of forcing the flow is different from, but entirely equivalent to, that used by, for example, Coceal *et al.* (2006), who imposed a fixed pressure gradient so that the flow rate (rather than the overall pressure gradient) varied with time. The Navier–Stokes equations were discretized in an orthogonal coordinate system using the staggered central second-order finite difference approximation. Advancement in time was achieved with a hybrid low-storage third-order Runge–Kutta scheme, using a fractional-step method with viscous terms treated implicitly and convective terms explicitly. The large sparse matrix resulting from the implicit terms was inverted by an approximate factorization technique and, at each time step, the momentum equations were advanced with the pressure from the previous time step, yielding an intermediate non-solenoidal velocity field ($\hat{\boldsymbol{u}}$), which was corrected to the required divergence-free solution by using a scalar quantity to project it onto a solenoidal field (see Kim & Moin 1985). As noted earlier, the surface roughness (arrays of cubes in this case) was treated using an efficient immersed boundary technique, which allows solution over complex geometries without the need for intensive body-fitted grids. This consists of imposing $U_i = 0$ on the body surface, which does not necessarily coincide with the grid. To avoid the geometry being described in a stepwise way, at the first point outside the body the second derivatives in the Navier–Stokes equations are discretized using the distance between the velocity points and the boundary of the body rather than using the mesh size. Full details of the numerical schemes can be found in Orlandi (2000) and Orlandi & Leonardi (2006).

Figure 1 shows the x–z computational domain for (two of) the surfaces. The plan area density λ_p is defined as the plan area of the cubes divided by the total plan area. The figure shows the cases $\lambda_p = 0.25$, the subject of considerable earlier experimental and numerical work (e.g. Cheng & Castro 2002: Coceal *et al.* 2006) and $\lambda_p = 0.11$. Note that in every case the cubes are lined up in the spanwise direction, but staggered in the axial direction and with each cube positioned centrally between the two nearest upstream cubes. There are, of course, numerous other possible arrangements of staggered patterns which would yield the same λ_p, but this one is the most symmetric. Note also that the cube size is the same in each case and, because they are cubes, the frontal area density λ_f (frontal area divided by total plan area) is the same as λ_p. Only use of non-cubic blocks would allow $\lambda_f \neq \lambda_p$, but the parameter space would then become very large. The minimal 'repeating unit' is identified in the figure; the

https://doi.org/10.1017/S002211200999423X Published online by Cambridge University Press

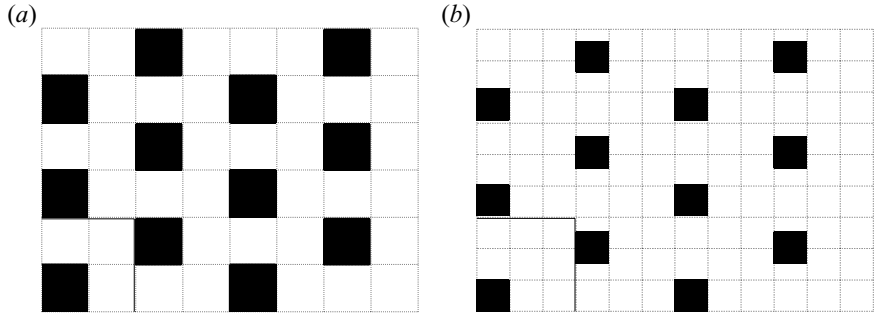


FIGURE 1. Geometrical configuration. Each cube has the same size; the differences in the figures are due to the different extent of the computational boxes. (*a*) Plan density $\lambda_p = 0.25$ (1:4); (*b*) $\lambda_p = 0.11$ (1:9). The thick line denotes the minimal repeating unit of which there are 12 in each case.

DNS domain contains four of these in the axial and (with one exception) three in the spanwise directions, although some computations were also done with larger spanwise and/or axial domains. In terms of cube height h the axial and spanwise domain widths therefore varied between $L_x = 8h$, $L_z = 6h$, respectively, for $\lambda_p = 0.25$, to $L_x = 12h$, $L_z = 9h$ for $\lambda_p = 0.11$. For the case of the smallest λ_p (0.04), the domain width covered only two repeating units ($L_x = 10h$, $L_z = 10h$). It should be emphasized that the domain length is not sufficient to allow development of single identifiable structures of very long axial extent. Typical spatial correlation coefficients of the axial fluctuating velocity did not always fall below about 0.3 over half the length of the (periodic) domain. However, Coceal *et al.* (2006) showed for the $\lambda = 0.25$ case that even restricting the axial length to $4h$ rather than (the present) $8h$ led to no discernible changes in the mean flow statistics, or even the second-order quantities like the turbulence stresses. The present domain lengths ($8h \leqslant L_x \leqslant 12h$) are thus adequate for our purposes.

As in Coceal *et al.* (2006) periodic conditions were applied in the streamwise and spanwise directions and a free-slip condition ($\partial u/\partial y = v = 0$) was imposed at the upper boundary, which was at $y = H = 8h$ where $y = 0$ is at the bottom wall. This allowed us to compute a 'half-channel' with fewer computational resources, but note that the flow near the upper boundary is not strictly identical with that on the symmetry axis of a full channel (with cubes on both walls), because in that case symmetry only occurs in the mean. No-slip conditions were applied on all solid surfaces. The Reynolds number was $Re = U_b h/\nu = 7000$ which led to typical Reynolds numbers based on the friction velocity u_τ of around 600 (i.e. $u_\tau H/\nu \approx 4800$), similar to the 500 imposed by Coceal *et al.* (2006) in their computations. As indicated in § 1 the dependence on Reynolds number in these flows is weak – largely because the surface drag is predominantly form drag (see Xie & Castro 2006 for further discussion of this point). In their boundary layer laboratory experiments, Cheng & Castro (2002) found little variation in the drag for Re between about 5000 and 12 000. Most of their measurements had $\delta/h = 7.5$, where δ is the boundary layer thickness. Coceal *et al.* (2006) showed that their own more limited domain height ($H = 4h$) did not constrain the flow below about $z = 3.5h$, with data in the canopy and roughness sublayer regions agreeing well with experimental data obtained in a boundary layer. The present computations might therefore be expected to yield flows in these regions very close to those that would occur in a developing boundary layer, provided the boundary layer depth is not too different from $8h$.

https://doi.org/10.1017/S002211200999423X Published online by Cambridge University Press

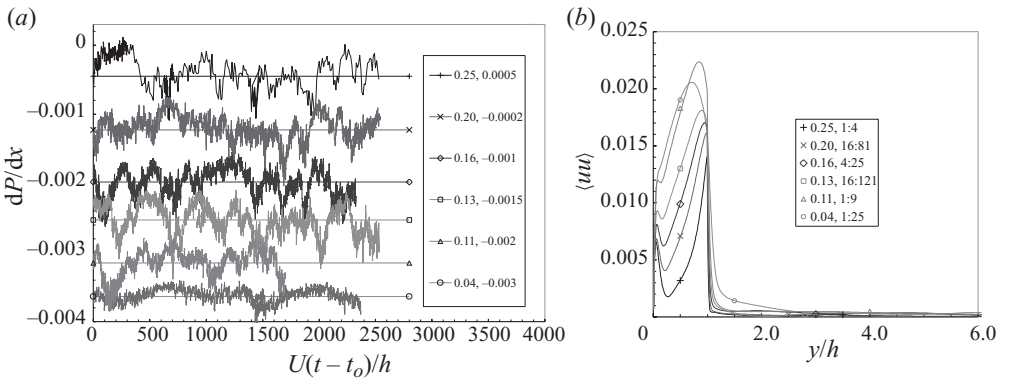


FIGURE 2. (*a*) Pressure gradient histories; traces shifted vertically for clarity; legend identifies values of λ_p and the vertical offsets of the time traces. (*b*) Dispersive stresses for the axial component; legend shows λ_p and the corresponding number of cubes per repeating unit plan area. Both figures show raw (unnormalized) data.

Three hundred and twenty grid nodes were used in the vertical, with 100 uniformly spaced nodes over the height of the cubes. Mesh sizes in the other two directions were always $h/32$, yielding typically about 35 million nodes within the domain. Ratios of the vertical grid size to the Kolmogorov length scale nowhere exceeded about five. The grid corresponds to even better (vertical) resolution than that used by the simulations of Coceal *et al.* (2006) at similar Re – they demonstrated that in their computations the major part of the dissipation spectrum was resolved. We are therefore confident that the present simulations are well resolved, not least in terms of obtaining reasonably accurate estimates of the frictional drag, which requires accurate determination of the wall-normal velocity gradients on all solid surfaces.

All computations were initiated with uniform velocity everywhere and had start-up run periods of at least $500T$, where T is a global time scale given by $T = h/U_b$. Subsequent averaging times were at least $2000T$ in nearly all cases. These times are both a little smaller than used by Coceal *et al.* (2006) but generally turned out to be adequate for obtaining converged statistics. A major issue, however, concerns the presence in some cases of spanwise inhomogeneities caused by large-scale longitudinal 'rolls', which could periodically appear and disappear over quite long time scales. If the averaging time is too short (or does not capture an integral number of these periodicities) dispersive stresses arising from spatial inhomogeneities caused by the rolls are significant in the region above the canopy layer, as shown also by Coceal *et al.* (2006). The relatively large time-scale variations in the flow can be seen in, for example, the time traces of the overall pressure gradient, which are shown in figure 2(*a*). Only for the smallest plan area density ($\lambda_p = 0.04$) are, arguably, such variations absent. They seem to be most evident in the $\lambda_p = 0.13$ case, but there is no obvious reason why this should be so. Typically, the oscillation time periods are between about 200 and 500 non-dimensional time units; this is large and it is clear that too short an averaging time would lead to inadequate statistics. In the absence (on average) of large longitudinal rolls, one expects the dispersive turbulence stresses – i.e. those that arise from spatial inhomogeneities in the mean flow – to be small above the canopy region, as discussed by Coceal *et al.* (2006). Figure 2(*b*) shows, as an example, vertical profiles of the (un-normalized) axial dispersive stress and in most cases it is indeed very small for $y/h > 1$. Within the canopy, dispersive stresses are

https://doi.org/10.1017/S002211200999423X Published online by Cambridge University Press

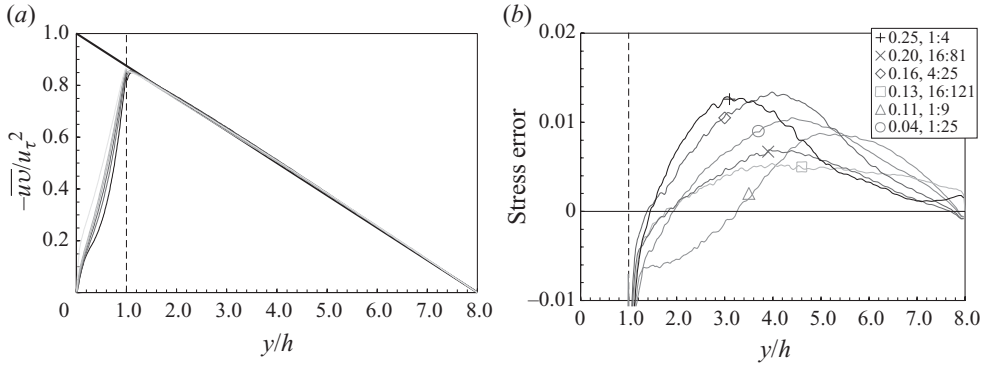


FIGURE 3. Spatially averaged turbulence shear stress: (*a*) normalized by total wall stress, with all six cases undistinguished and the bold straight line showing the expected total stress; (*b*) the difference between the computed turbulence stress and the expected (linear total) stress, with each case distinguished using a single symbol placed on the profile. Normalization is the same as in (*a*).

inevitably significant and are discussed briefly in § 4. As a further demonstration that the averaging times were in all cases sufficient, figure 3 presents the spatially averaged Reynolds shear stress ($-\overline{uv}$) profiles for all cases, normalized by the total wall stress which was computed as explained in § 3.1.1. One expects the usual turbulence shear stress, $-\overline{uv}$, to be close to the total shear stress, which must vary linearly (compare the straight bold line in figure 3*a*). It is clear that in all six cases the computational data have the expected behaviour and, in figure 3(*b*), the difference between the sum of the turbulence and viscous stresses and the expected linear total stress is shown. (The viscous shear stress was found to be below 0.5 % of the Reynolds stress over the bulk of the flow above the canopy.) In no case do the differences exceed about 1.2 % (for $y/h > 1.0$). Too short an averaging time would, however, lead to much larger errors than those shown in figure 3(*b*).

3. Results and discussion

3.1. *The mean flow*

3.1.1. *Deductions from mean velocity profiles*

The two common ways of writing the mean velocity log-law profile for a fully rough surface are

$$U^+ \equiv \frac{U}{u_\tau} = \frac{1}{\kappa}\ln y^+ + B - \Delta U^+ = \frac{1}{\kappa}\ln\left(\frac{y}{y_o}\right), \tag{3.1}$$

where ΔU^+ is usually termed the roughness function. This is zero for a smooth surface but generally increases with increasing roughness. Note that $\Delta U^+ = f(y_o u_\tau/\nu)$ only (strictly, $f(y_o u_\tau/\nu, B, \kappa)$) and that y_o, the roughness length, essentially encapsulates all the various geometrical details of the roughness geometry. Note also that in (3.1), and henceforth, it is to be understood that y has been reduced by the zero-plane displacement d. This was initially determined for every case in the usual way, i.e. by assuming there would be a logarithmic region in the spatially averaged mean velocity profiles and adjusting d to yield a straight line in the log-linear plot of U versus y whose slope (u_τ/κ) matched the value expected from the wall stress and a given value of κ (0.41). The wall stress was obtained independently of mean velocity profiles by

https://doi.org/10.1017/S002211200999423X Published online by Cambridge University Press

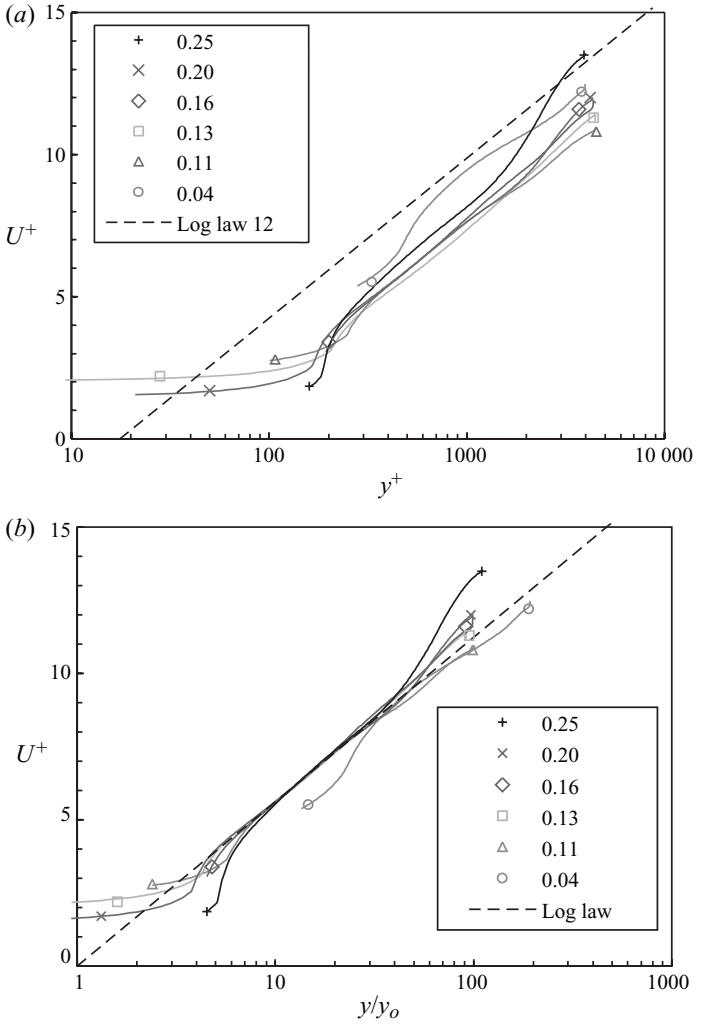


FIGURE 4. Spatially averaged mean velocity profiles. Plotted against y^+ (a) and y/y_0 (b). The symbols are located near the end of each curve to which they refer. In (a) the usual log-law line, $U^+ = (1/\kappa)\ln y^+ + B$ has B (normally 5) reduced by 12, for clarity.

computing the sum of the time-averaged form drag on all cubes in the domain and the total frictional drag on all horizontal surfaces; it could also be computed directly from the time-averaged longitudinal pressure gradient and, for all cases, the difference in u_τ obtained from these two methods was below 1 %.

We consider first the way in which changes in λ_p affect the spatially averaged mean velocity profiles. These are shown in figure 4. With the usual inner layer scaling (figure 4a) the profiles all fall well below the standard log-law line, as expected, with values of ΔU^+ reaching a peak of around 14.5. Note that to emphasize the variations in roughness function from case to case, B in figure 4(a) has been taken (arbitrarily) as -7, rather than the usual 5, moving the dashed line conveniently close to the computed profiles. For $\lambda_p = 0.04$, d is very small and any possible log-law region occurs well above the cube's crest plane (around $y^+ = 500$)

https://doi.org/10.1017/S002211200999423X Published online by Cambridge University Press

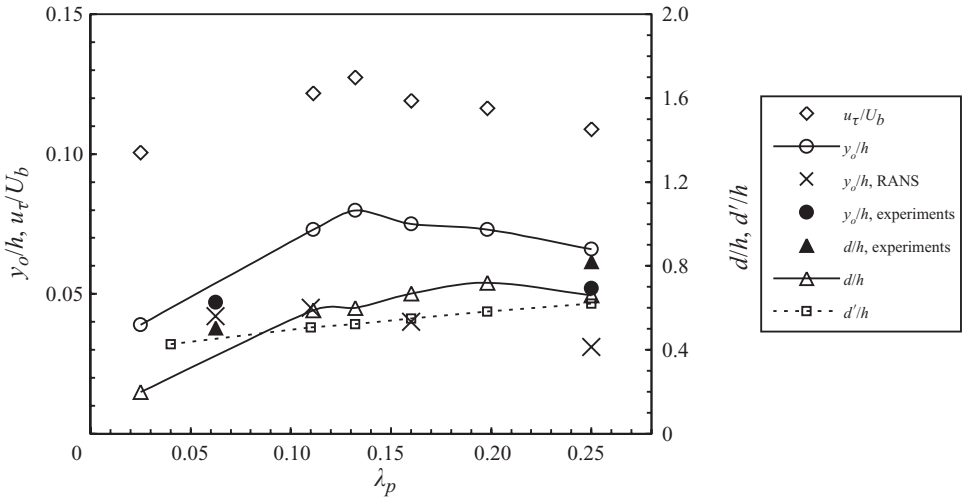


FIGURE 5. Variations of y_o/h and u_τ/U_b (left-hand ordinate), and d/h and d'/h (right-hand ordinate) with λ_p. The solid symbols are from the boundary layer experiments of Cheng *et al.* (2007) and the crosses are from the RANS computations of Santiago *et al.* (2008).

but ΔU^+ is still in excess of 12. Individual profiles at particular (x, z) locations do not, of course, necessarily have a log-law shape inside the roughness sublayer – the region within which the mean flow is spatially inhomogeneous in the horizontal. The top of this region is around $y/h = 1.5$, judged by the approximate convergence of individual turbulence stress profiles, and all log-law fits have taken this height as a lower limit. It should be emphasized that there is no *a priori* reason to expect the appearance of a log-law region in the 'spatially averaged' profiles below this height, unless one accepts that the usual matching or mixing length arguments hold in a spatially averaged sense. The particular, rather extreme case – of just one cube in an area equal to 25 times its own plan area ($\lambda_p = 0.04$) – might more properly be regarded as flow over an isolated bluff body, rather than a genuine rough-surface flow. There are much more convincing log-law regions in all other cases, as emphasized in figure 4(*b*), which shows the profiles plotted using the more appropriate y_o scaling (the far right-hand side of (3.1)). Close inspection of figure 4(*a*) indicates that ΔU^+ rises to a maximum as λ_p increases before falling again; the corresponding variation in y_o which produces the collapse in figure 4(*b*) is shown in figure 5. This figure also includes the variations in zero-plane displacement, which are discussed in due course.

Figure 5 suggests that the area density leading to the peak y_o is around 15 %. It could be argued that the 'roughest' surface is the one that produces the highest wall stress (thus requiring the largest axial pressure gradient) for a given bulk flow rate. The figure includes the friction velocity data and shows that their variation is broadly similar to that of y_o. Leonardi *et al.* (2003) found a similar correspondence between u_τ and ΔU^+. (Recall that the bulk velocity U_b is kept fixed throughout the computations; variations in ρu_τ^2 from case to case correspond to variations in the time-averaged pressure gradient.) Only if the log law were obeyed all the way between $y = y_o$ and $y = H$ would u_τ/U_b be expected to change monotonically with y_o/h. As in a smooth-wall channel flow, the log-law region does not in fact cover the entire domain height, so it would not be surprising if there were a small mismatch between

https://doi.org/10.1017/S002211200999423X Published online by Cambridge University Press

the λ_p values for maximum y_o and maximum u_τ (although in fact figure 5 suggests that this is insignificant). We can conclude that the plan area density which yields maximum surface stress (and thus drag and, roughly, y_o/h) is around 15 %; in the context of boundary layer flows it seems unlikely that this result will vary significantly with, say, δ/h where δ is the boundary layer depth.

This range of λ_p for maximum roughness effect is very close to that found by Kanda *et al.* (2004) for a square array of cubes, using LES. It is also similar to the range deduced from the predictions of Santiago *et al.* (2008) (see figure 5), who used a standard RANS model. However, the latter showed that the values of some quantities (like the sectional drag coefficient, see below) when computed using RANS are larger than the DNS results by around a factor of 2, which must be largely a result of the inadequacies in the standard k-ϵ turbulence model used for the RANS computations, some of which were noted by Santiago *et al.* Figure 5 also includes experimental data obtained by Cheng *et al.* (2007) in a boundary layer. The agreement is satisfyingly close to the present results, especially given the well-known uncertainties in the fitting procedures required to obtain both quantities – particularly in boundary layers for which u_τ has also to be obtained in some independent way.

Hagishima *et al.* (2009), in wind tunnel boundary layer experiments over various surfaces, found for the staggered cube array with $\lambda_p = 0.25$ a value of y_o/h similar to the present value. Like Cheng *et al.* (2007) they obtained the surface drag directly using a force balance, which should provide a more accurate measure of u_τ and in that sense is equivalent to channel calculations in which u_τ is also known independently. On the other hand, Macdonald (2000) reported y_o/h values from boundary layer experiments over the same surface and his results (not shown here) are higher than the present data (and those of Cheng *et al.* 2007) and they also suggest a peak y_o/h at a rather higher value of λ_p (about 0.18). However, although he used a more sophisticated method of estimating the three parameters $(y_o/h, d/h, u_\tau)$ from the velocity profiles, as discussed in Macdonald, Griffiths & Hall (1998), he used neither an independent estimate of u_τ nor spatially averaged velocity profiles – both of which are available only in the experiments of Cheng *et al.* (2007) and the present DNS (and Coceal *et al.* 2006). The differences are therefore perhaps not surprising, although it is interesting that the resulting values of y_o/h are about a factor of 2 higher than those in figure 5 (see below).

As mentioned earlier, the zero-plane displacement d was found in the usual way by optimizing the fit of the spatially averaged mean velocity to the log-linear profile (2), assuming $\kappa = 0.41$ and using the known wall stress to compute u_τ. As expected, it rises with increasing λ_p, as evident in figure 5. For large enough λ_p it would eventually reach a value near unity, of course, since once $\lambda_p = 1$ the flow would revert to a smooth wall channel of half-depth $7h$. Coceal *et al.* (2006) argued that in a channel the proper friction velocity to be used in the log law (u^*, say) should be reduced from u_τ by the factor $\sqrt{1-h/H}$, accounting for the expected linear variation in stress from $y = d$ to the centreline (see figure 3*a*). More consistently, one should use the factor $\sqrt{1-d/H}$. In the present case the difference between u^* and u_τ is less than 4 %; the consequent changes in y_o (around a 15 % decrease) do not change the trends shown in figure 5 and, in addition, the log-law fit was not significantly improved. The resulting d/h values, like those of Hagishima *et al.* (2009) and Cheng *et al.* (2007), are significantly higher than those of Macdonald's measurements (Macdonald 2000) or his model (Macdonald *et al.* 1998); as in the case of y_o/h this must be a result of uncertainties in trying to estimate all three parameters – u_τ, y_o and d. Constraining u_τ by obtaining it independently of mean velocity profiles is inherently a much more satisfactory procedure.

https://doi.org/10.1017/S0022112009994423X Published online by Cambridge University Press

However, we do not believe that the zero-plane displacement height d should be viewed merely as an additional fitting constant. Like y_o, it must clearly depend on (probably all) the various geometric features of the roughness and it is surely better to seek a physically based definition for it, even though it is probably not possible to relate it in some analytic way to these various features, which some authors in the meteorological field have sought to do. In fact, Jackson (1981) demonstrated rigorously that the zero-plane displacement should properly be thought of as the height at which the total drag acts or, equivalently, the mean level of momentum absorption by the surface. This can be expressed by

$$d' = \int_0^h yD(y)\mathrm{d}y \Big/ \int_0^h D(y)\mathrm{d}y, \tag{3.2}$$

where $D(y)$ is the sum of all forces acting at height y. The denominator in (3.2) is thus the sum of all forces, whether from axial pressure differences across the cube or frictional forces on the cube faces and the bottom surface. So, in principle, d' is a fluid dynamical property of the surface, which must satisfy dimensional constraints similar to those on y_o. (Note that, unlike d or d', y_o does not influence the velocity gradient.) For the present case, it is thus of interest to compute the height as defined above and compare it with the value of d necessary to achieve a good log-law fit given the usual value of κ. Figure 5 includes the resulting d' data and, except at the lowest λ_p, they are a little below the values of d. Although not very large (typically about 20 %), the difference is very significant; using d' in the log-law expression does not yield a sensible fit to the mean velocity data. Jackson's arguments (Jackson 1981) depend crucially on the reasonable assumption that the inertial sublayer does not depend on the detailed morphology of the surface except for the height at which the (axial) drag force acts. A possible implication of the present results would thus be that this assumption does not hold. An alternative possibility, however, is that von Kármán's coefficient is not universal, but depends on the nature of the surface, as discussed in § 1. Pursuing this possibility for the $\lambda_p = 0.25$ case as an example, using d' instead of d and $\sqrt{1 - d'/H}u_\tau$ instead of u_τ (see above), the value of κ required to produce a good log-law fit is 0.36. The fit is then in fact marginally (and in some of the other cases significantly) better than that shown in figure 4(b). Doing the same analysis for all cases leads to the data shown in figure 6(a), which suggests that values of κ vary between 0.41 and 0.36 as λ_p increases. The values of y_o are now about a factor of 2 higher than previously and the peak in y_o occurs around $\lambda_p = 0.17$ – a little higher than suggested by the data in figure 5.

The present data are almost unique for cases in which d is certainly 'not' zero, in that they supply accurate determination of d on the basis of Jackson's physically appealing definition (Jackson 1981). They seem to confirm that, indeed, κ varies depending on the nature of the surface, as suggested by some of the atmospheric data mentioned in § 1. Some additional evidence for surfaces of the present kind can be adduced from the work of Kanda *et al.* (2004), who undertook LES of flow over square in-line (rather than staggered) arrays of cubes. They found that use of d' – which, like the present data, was significantly lower than d – led to 'no acceptable fitting log-law region' for any λ_p. The same conclusion was reached by Cheng *et al.* (2007), who deduced surface drag from both a floating balance and surface pressure data, for boundary layers over staggered cube arrays ($\lambda_p = 0.0625$ and 0.25). But both these authors used a fixed value of κ and their data would have been well fitted by a log law if κ had been chosen appropriately. Indeed, the Cheng *et al.* (2007) data,

https://doi.org/10.1017/S002211200999423X Published online by Cambridge University Press

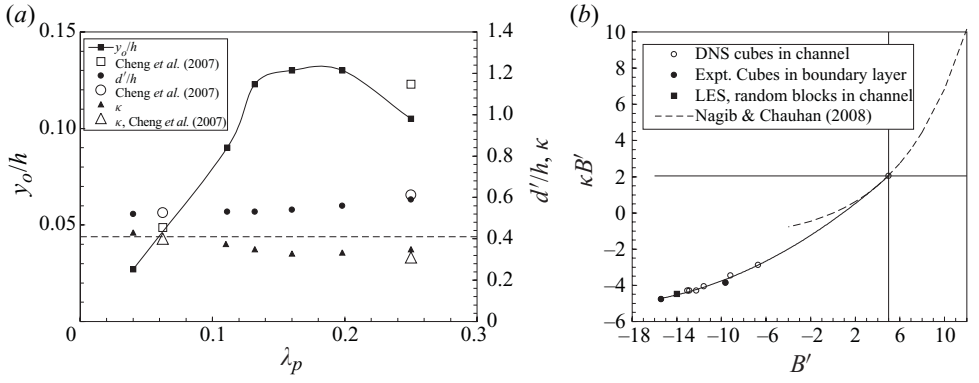


FIGURE 6. (*a*) Variations of y_o (squares), d' (circles) and κ (triangles) with λ_p, obtained from log-law fits. Open symbols are from the boundary layer experiments of Cheng *et al.* (2007). (*b*) $\kappa B'$ versus B', compared with a polynomial fit through the data (solid line) and with the curve fit of Nagib & Chauhan (2008) through a large assembly of smooth-wall data (dashed line).

reworked using d', is included in figure 6(*a*) and is seen to be entirely consistent with the present DNS data.

Figure 6(*b*) shows the resulting values for $\kappa B'$ (with $B' = B - \Delta U^+$) in the form presented by Nagib & Chauhan (2008). They claim that κ in zero-pressure-gradient boundary layers (at sufficiently high Reynolds number) is 0.384 whereas in planar channels and in pipes it is $\approx$0.37 and 0.41, respectively. They collected a whole range of smooth-wall high-quality high-Reynolds-number data from pipes, channels and boundary layers, including those under various favourable or adverse pressure gradients, and showed that the product κB does not vary linearly with B, the additive constant in the log-law relation, as it would if κ were constant. Rather, κB varies nonlinearly with B; the zero-pressure-gradient boundary layer, the two-dimensional channel and the pipe cases appear as single but separate points on the curve, with other points coming from variable pressure gradient cases. Figure 6(*b*) includes data from the Cheng *et al.* (2007) experiments and the LES of Xie *et al.* (2008) for channel flow over roughness elements of random height. It is evident that the data are fitted best by a polynomial rather than linear curve and that this curve provides a reasonable continuation of (much of) Nagib and Chauhan's curve fit (Nagib & Chauhan 2008) for smooth-wall data – with the exception of the high adverse pressure gradient data which provides values of B between about -1 and -4. (For smooth walls, $\Delta U^+ = 0$, of course.)

By writing $\kappa y = u_\tau^3/(u_\tau^2 \partial U/\partial y)$ (from the log law) it is possible to argue rather loosely that any change in the 'dissipation deficit' – i.e. the amount by which the dissipation does not balance the production of turbulence kinetic energy in the log-law region – will inevitably change κ (Vogel & Frenzen 2002). It is known that large roughness tends to make the turbulence more isotropic and this is quite likely to change the production/dissipation ratio, as indeed do significant pressure gradient effects in smooth-wall flows. We return to this point in § 4.

3.1.2. *Pressure and frictional drag*

It is of interest to consider how much of the surface stress is provided by frictional drag on the $y = 0$ surface and on the cube tops (and sides), compared with the

https://doi.org/10.1017/S002211200999423X Published online by Cambridge University Press

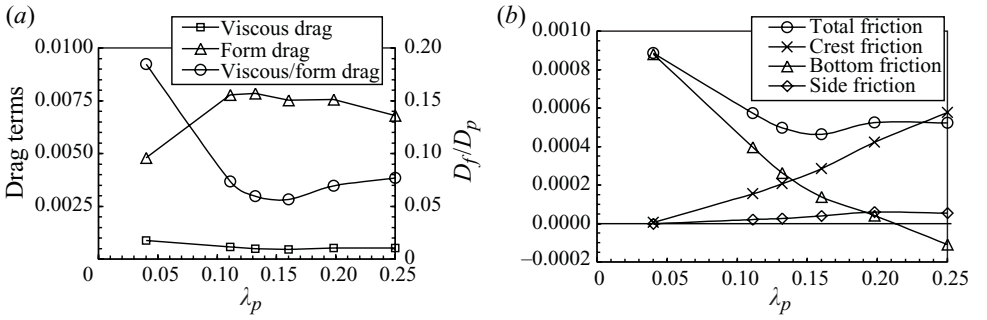


FIGURE 7. (*a*) Form (D_p) and total frictional (D_f) drag, and their ratio (right hand ordinate); (*b*) bottom (D_b), crest (D_c), side (D_s) and the total frictional drag (D_f).

proportion arising from pressure (i.e. form) drag, not least because this would indicate the likely Reynolds number sensitivity in the results (e.g. for u_τ). As mentioned earlier, a common assumption is that the frictional components are negligible, at least for sufficiently large λ_p. The frictional drag D_f was obtained directly from the present results by summing the usual expression for wall stress ($\mu(\partial U/\partial y)|_o$) over all the $y=0$ and $y=h$ surfaces, and similarly for the side surfaces. Likewise, defining $\Delta p(y)=\frac{1}{h}\int_{span}[\overline{p_f}(y)-\overline{p_b}(y)]\mathrm{d}z$ as the (time-averaged and) laterally integrated front-to-back pressure difference across a cube at height y, the form drag D_p was found by summing over the height of the cube, so that for the entire domain surface $D_p=(\lambda_p/h)\int\Delta p\mathrm{d}y$. Note that $D_f+D_p=\rho u_\tau^2$. The frictional drag can be further subdivided into three contributions: one arising from friction at $y=0$, D_b say, one associated with the flow at the cube crests ($y=h$), D_c say, and one for the cube sidewalls, D_s say, so $D_f=D_b+D_c+D_s$. Figure 7 shows how these various contributions to the total drag force vary with λ_p. It is clear from figure 7(*a*) that the frictional drag is a minimum at about 5 % of the form drag for $\lambda_p\approx 0.16$, with roughly equal contributions from bottom and crest friction (figure 7*b*). However, it naturally becomes much larger for less dense arrays when, although the influence of crest friction becomes negligible, there is a significant increase in bottom friction. On the other hand, for much denser arrays, the crest friction (D_c) actually rises above the total friction, because the recirculating regions between the cubes become a more dominant feature of the inter-cube flow and make a negative contribution to the total friction – see figure 7(*b*) at $\lambda_p=0.25$. For even larger λ_p, the magnitude of the bottom friction must eventually fall again, with the crest friction providing all the surface drag since the form drag must also tend to zero: i.e. as $\lambda_p\to 1$, $D_f\to D_c$, $D_b\to 0$ and $D_p\to 0$. Figure 7(*b*) suggests that the crest and side friction contributions may become negative for small enough λ_p (lower than 0.04). This is entirely possible and would be associated with the significantly larger reversed flow region on the top and side surfaces of more isolated cubes.

It is worth emphasizing here that it would not be possible to obtain data of the kind shown in figure 7 using RANS methods, for none of the current wall-law formulations are appropriate for the flows near any of the solid surfaces. Likewise, regular LES computations would in principle be problematic in this respect also, unless very sophisticated near-wall treatments were implemented. On the other hand, since the frictional contribution to total surface stress is below about 7 % provided $0.1<\lambda_p<0.25$, inadequate wall treatments would not necessarily seriously degrade

https://doi.org/10.1017/S002211200999423X Published online by Cambridge University Press

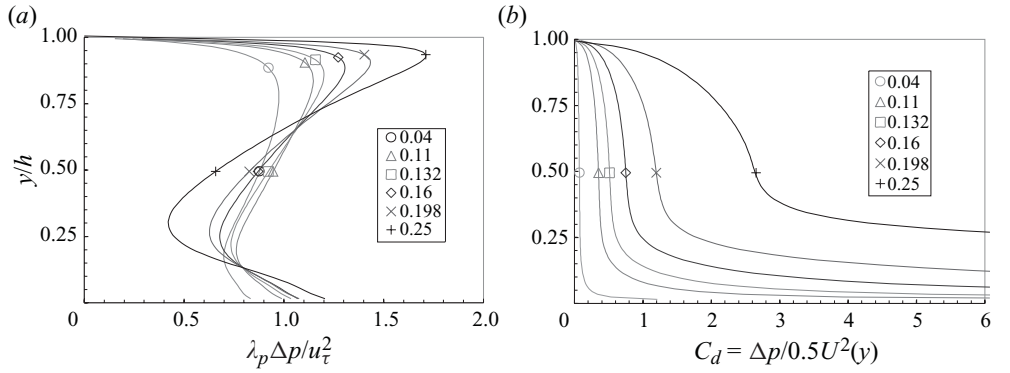


FIGURE 8. Variations of normalized pressure difference (a) and sectional drag coefficient (b). Symbols identify each curve, with corresponding values of λ_p in the legends.

LES computations of the overall flows in this range of λ_p (as argued by Xie & Castro 2006).

A number of authors have discussed how best to normalize D_p to produce an appropriate drag coefficient. This is particularly important for the class of urban canopy models which treat the urban area as a porous medium modelled in terms of a drag force distributed in height (as in, e.g. Coceal & Belcher 2004). In such models, a 'sectional' drag coefficient, $C_d(y)$ say, is needed. This requires knowledge of the vertical distribution of both the drag force ($\Delta p(y)$) and the spatially averaged flow variables that can be used to provide an appropriate velocity scale – at least the mean velocity and perhaps also other quantities, like the turbulence kinetic energy. These are extremely difficult, if not impossible, to obtain from field or laboratory experiments but it is straightforward to deduce them from computational data. Figure 8 shows the variation with height of the laterally integrated pressure difference across the cube, $\Delta p(y)$, for all cases. In figure 8(a) the data are normalized using u_τ^2/λ_p, so that if frictional drag were zero the integral over the height of the cube would be exactly unity. It is clear that as the areal density decreases the peak-to-peak variation in the sectional pressure difference falls significantly. So, for example, whilst it is 1.3 for $\lambda_p = 0.25$ it is only about 0.2 for $\lambda_p = 0.04$; in the latter case the frictional contribution is significant, so the integrated value of $\lambda_p \Delta p/u_\tau^2$ is only about 0.81. In all cases the largest contribution to the form drag arises from the upper half of the cubes, principally because the mean velocity is highest there. In fact, in every case the spatially integrated mean axial velocity over $0.5 < y/h \leqslant 1.0$ is around 80 % of the value integrated over the whole cube height; it is interesting that this figure is largely independent of λ_p. Note that these results are consistent with the finding that for arrays of random (or at least multiple) height obstacles, the surface stress is dominated by the form drag of the tallest obstacles (see Kanda 2006; Xie *et al.* 2008).

Figure 8(b) shows the sectional drag coefficient, defined by $C_d(y) = \Delta p/(1/2)U(y)^2$, as a function of height for each value of λ_p. The data emphasize the difficulty with this definition, arising because $U(y)$ becomes very small in the lower regions of the flow and may even become negative. (Recall that $U(y)$ is the horizontally averaged velocity. For $\lambda_p = 0.25$ the recirculating flow behind each cube is sufficiently extensive within the inter-cube regions to lead to a change of sign in $U(y)$.) The consequent difficulty of parameterization in the urban canopy models mentioned above has led some authors to consider alternative normalizations. Martilli & Santiago (2007), for

https://doi.org/10.1017/S002211200999423X Published online by Cambridge University Press

example, defined a modified drag coefficient as

$$C_{d\,mod}(y) = \frac{2\Delta p(y)}{q_{tot}(y)}, \tag{3.3}$$

where q_{tot} is twice the total kinetic energy in the flow, which includes the contributions from the spatially averaged velocity, time fluctuations and spatial fluctuations from it. So $q_{tot}(y) = U(y)^2 + v_{tke}^2(y) + v_{dke}^2$, where v_{tke}^2 is twice the usual turbulence kinetic energy (i.e. the sum of mean squares of all three fluctuating velocity components) and v_{dke}^2, likewise, is twice the dispersive kinetic energy arising from the spatial fluctuations in the time-averaged mean velocity field. This definition recognizes that the mean velocity is not really an appropriate (or the only important) velocity scale in regions of high-turbulence intensity. Although $C_{d\,mod}(y)$ (not shown) varies much less significantly with height than $C_d(y)$, it would really only be a useful basis for parameterization schemes if the spatially integrated variations with height of the turbulence quantities were known *a priori*; this is not in practice ever the case so we do not pursue discussion of $C_{d\,mod}(y)$ here. It is worth noting, however, that although the values of $C_d(y)$ are seriously overpredicted by RANS methods (shown by Santiago *et al.* 2008, for $\lambda = 0.25$), the present data suggest that height-averaged values of $C_{d\,mod}(y)$ are relatively close to those obtained by Santiago *et al.* using RANS. This seems to be an example of how RANS can sometimes give reasonable results but only because of the counterbalancing of large errors. These may arise, in the $k-\epsilon$ model for example, from inadequate modelling of various terms in the energy and/or dissipation equations, combined with inappropriate use of an eddy viscosity model.

4. The turbulence field

We confine ourselves largely to consideration of the turbulence stresses. Figures 9(*a*) and 9(*b*), respectively, show profiles of the spatially averaged normalized axial ($\overline{u^2}^+$) and vertical ($\overline{v^2}^+$) normal Reynolds stresses for each case. The figures include the smooth-wall channel flow data of Moser, Kim & Mansour (1999), for a Reynolds number $u_\tau H/\nu = 587$, where H is the channel half-width. The wall distance for this latter data has been scaled so that $y/h = 1$ corresponds to the smooth-wall location. The first observation is that once $y/h > 2$ the present rough surface results neither vary very much amongst themselves nor are significantly different from the smooth-wall data. (Note, however, that since the present outer boundary condition – free slip – differs from that of Moser *et al.*, who computed the entire channel depth, the vertical stress behaviour is necessarily different near that outer boundary.) Data from a boundary layer at moderate Reynolds number are also included. These are plotted at $y/h = 2$ and show the range of data obtained by Erm & Joubert (1991) for wall distances within $0.1 < y/\delta < 0.3$ – i.e. roughly within the log-law region. Again, there is little difference between these data and the present data a little above the top of the canopy. Not surprisingly therefore the structural parameters $\overline{v^2}/\overline{u^2}$ and $-\overline{uv}/k$, where k is the total turbulence kinetic energy, are also very similar to those in the smooth-wall flows (see figure 10 discussed below).

It thus seems that the roughness does not affect the basic turbulence features of the outer flow, in conformity with Townsend's hypothesis that the only effect of roughness is to change the surface stress. Given the relatively large size of the roughness in the present case, this is perhaps a little surprising. It is also in direct contrast to the findings of Bhaganagar *et al.* (2004) who, from DNS of a channel flow with one

https://doi.org/10.1017/S002211200999423X Published online by Cambridge University Press

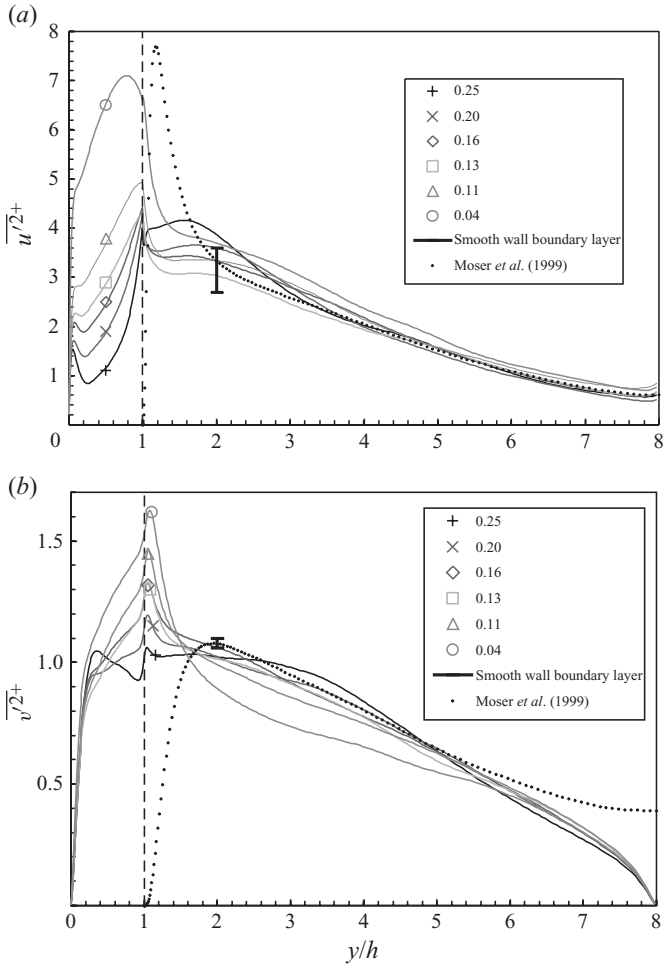


FIGURE 9. Reynolds stresses: (*a*) $\overline{u^{2+}}$; (*b*) $\overline{v^{2+}}$. Values of λ_p in the legends with symbols identifying each curve. Smooth-wall boundary layer data (at $y/h = 2$) is for $0.1 < y/\delta < 0.3$ from Erm & Joubert (1991).

smooth and one rough wall, showed that the appropriately normalized Reynolds stresses in the outer flow were significantly smaller on the rough-wall side. These computations used 'egg carton' type roughness, having smooth (three-dimensional) sinusoidal shapes. In addition, the roughness heights were very low (with equivalent sand grain roughness heights of $k_s^+ < 70$), so that the rough surfaces were in fact only transitionally rough. One might on that basis have expected only small effects in the outer flow. In contrast, and in agreement with the present data, Bakken *et al.* (2005) have shown that normal stresses in the outer region of channel flows with rod-roughened or mesh-roughened walls are very similar to smooth-wall data. But they suggested that 'levels of $\overline{v^{2+}}$ are much more connected to Reynolds number effects than to boundary conditions'. Computations for the present $\lambda_p = 0.25$ case at one half and one quarter of the original Reynolds number ($Re = U_b h/\nu = 7000$) showed noticeably smaller stresses in the outer region so this may indeed be the reason for the rather different behaviour found by Bhaganagar *et al.* (2004).

https://doi.org/10.1017/S002211200999423X Published online by Cambridge University Press

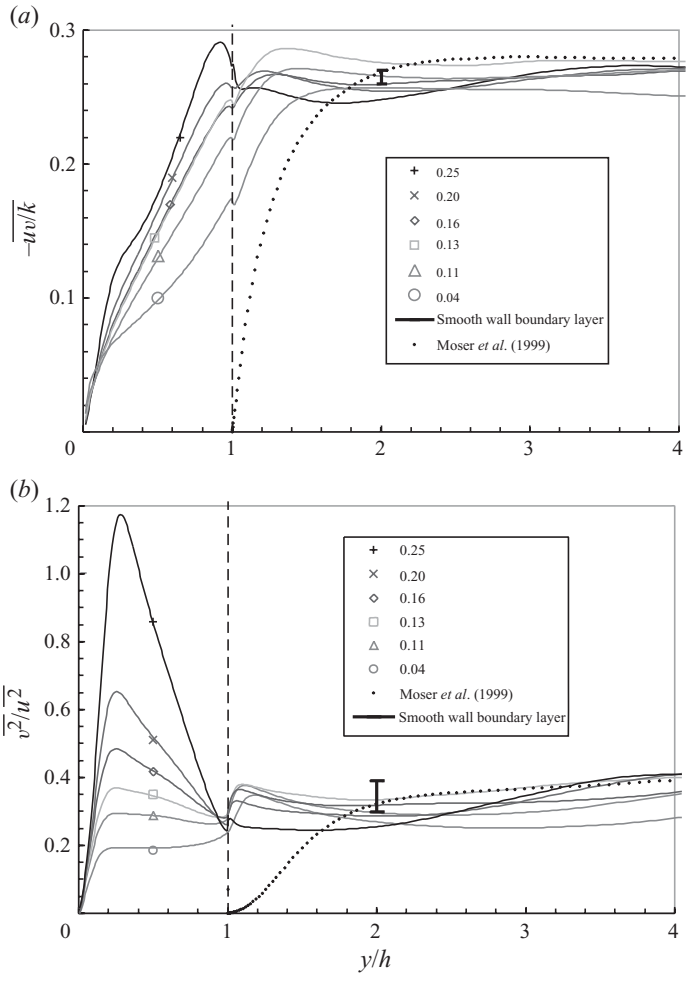


FIGURE 10. Structure parameters: (*a*): $\overline{uv}/k$; (*b*) $\overline{v^2}/\overline{u^2}$. Values of λ_p are given in the legends with symbols identifying each curve. Smooth-wall boundary layer data (at $y/h = 2$ is for $0.1 < y/\delta < 0.3$ from Erm & Joubert (1991).

Nearer the wall, there are of course very significant effects of surface morphology. Figure 9 shows that the normal stresses reach a peak just above the roughness crests ($y = h$) and these peaks fall with increasing roughness density. Likewise, within the roughness canopy ($y/h < 1$) these two stress components (and the spanwise stress, $\overline{w^2}^+$, not shown) are increasingly reduced as λ_p increases. These changes are emphasized in figure 10, which shows (in figure 10*a*) the ratio of Reynolds shear stress to total turbulence kinetic energy, $k = (1/2)(\overline{u^2} + \overline{v^2} + \overline{w^2})$, and (in figure 10*b*) the ratio $\overline{v^2}/\overline{u^2}$, within the lower half of the flow ($y/h < 4$). It is clear that with increasing λ_p the turbulence within the canopy becomes increasingly isotropic, in that axial and vertical normal stresses become more similar. On the other hand, the shear stress becomes larger compared with the turbulence energy. This often suggests an increase in the efficiency of turbulence production processes, but it should be remembered that in this region mean flow gradients are generally small and dispersive stresses, i.e. those which arise because of the spatial inhomogeneity, are significant (recall figure 2*b*);

https://doi.org/10.1017/S002211200999423X Published online by Cambridge University Press

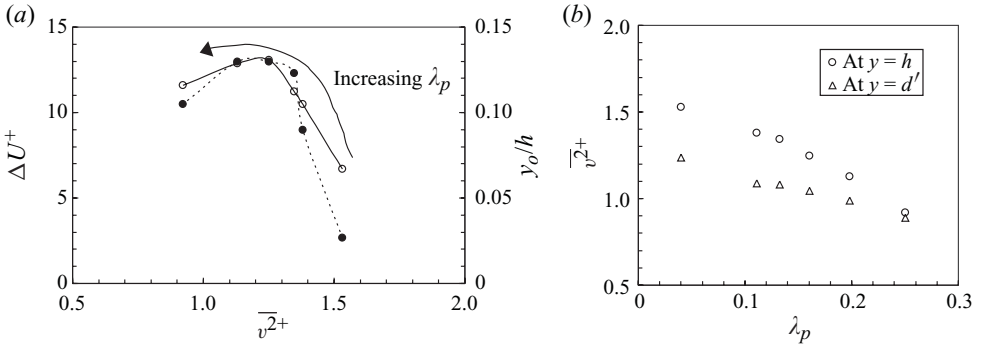


FIGURE 11. Variation of normal Reynolds stress at $y = h$ with roughness. (a) Open symbols: ΔU^+ versus $\overline{v^2}^+$; solid symbols: y_0/h versus $\overline{v^2}^+$. (b) $\overline{v^2}^+$ versus areal density λ_p.

typically the total dispersive kinetic energy is some 30 %–40 % of k. In view also of the high degree of three-dimensionality in the canopy flow, along with large spatial changes in mean flow direction, it would perhaps be better to consider principal stresses in any full discussion of the nature of the turbulence within the canopy.

One finding apparent from figures 9 and 10 should be particularly noted, as it is quite different from that found for two-dimensional roughness by Orlandi, Leonardi & Antonia (2006). They showed that the (spatially averaged) vertical stress at the crest plane increases monotonically with increasing roughness, both for longitudinal and transverse roughness ribs. In the present case, the reverse is true: figure 11(a) shows how $\overline{v^2}^+$ at the crest plane varies with the roughness function – measured by ΔU^+ or y_0/h. It is clear that for these three-dimensional roughness arrays the normal stress falls monotonically with increasing λ_p (figure 11b) although both the roughness function and roughness length have peaks around $\overline{v^2}^+ = 1.25$ (figure 11a). Similar plots of the normal stress at the zero-plane displacement height (d'), included in figure 11(b), or the peak value (just above the crest plane, not shown) have essentially the same behaviour. So in this respect the effect of roughness is entirely opposite to that found by Orlandi *et al.* for two-dimensional bar roughness. (Interestingly, they also found that for transverse bars the increase in normal stress appeared in the outer region too, whereas for flow-aligned bars it did not; the latter situation is in this respect similar to the present three-dimensional roughness where, as discussed earlier, the outer flow stresses are close to smooth-wall data.)

Finally, some comments on the ratio of production (P) to dissipation (ϵ) of turbulence kinetic energy are appropriate. Spatial averages of both P and ϵ were calculated from the DNS data using the exact, full relations. The ratio $|P/\epsilon|$ is in all cases significantly higher than unity within the log-law region. Just above the cubes it is around 2.8 falling to about 1.6 at the bottom of the log-law region (taken as $y/h = 1.5$) and then falling more slowly to a minimum between 1.1 and 1.4 (depending on λ_p). Average values within the log-law region and beyond thus vary somewhat with λ_p and are unequivocally higher than unity. This is in contrast to, for example, the data (at $Re_\tau = 590$) of Moser *et al.* (1999), which suggest $|P/\epsilon|$ values nearer 0.85 at the bottom of the log-law region, rising slightly to about 1.05. Such a significant excess of production over dissipation in the present cases is indicative of relatively large turbulence transport providing a higher sink of kinetic energy in the near-wall region than occurs in smooth-wall flows. Similar results have been found recently in the context of channel flow with two-dimensional roughness (e.g. Ikeda & Durbin 2007) and are well known in the context of atmospheric boundary layers (e.g.

https://doi.org/10.1017/S002211200999423X Published online by Cambridge University Press

Raupach, Finnigan & Brunet 1996; Finnigan 2000; Poggi *et al.* 2004). Changes in the kinetic energy balance, as suggested by Vengel & Frenzen (2002), may provide one of the underlying causes of changes in von Kármán's coefficient.

5. Concluding remarks

Mean flow and some basic turbulence parameters from direct simulations of channel flow with very rough walls comprising staggered arrays of cubes have been presented. Maximal surface drag (and thus wall roughness length) occurs when λ_p is around 15 %, in agreement with laboratory data from boundary layers growing over similar surfaces and also with computations using RANS or LES techniques. The former, however, significantly overpredict sectional drag forces on the roughness elements when compared with the present DNS data or, indeed, previous DNS and LES data for similar cases. In most cases studied here, the frictional component of the surface drag is no larger than about 7 %, consistent with the flows being only very weakly dependent on Reynolds number, in contrast to comparable smooth-wall flows. The sectional drag forces on the roughness have been shown to vary less as λ_p decreases but in all cases the upper part of the roughness contributes most to the form drag. RANS methods seriously overpredict sectional drag coefficients. In common with earlier laboratory and computational studies by various authors, it is evident that turbulent transport plays a significantly larger role in the surface layer than it does in smooth-wall flows, but details of the precise structural mechanisms causing this in the present cases remain to be explored. It is clear, however, that despite the relatively large roughness of the present flows, the turbulence Reynolds stresses in the outer layer are very similar to those in smooth-wall channel flows. This lends credence to the Townsend hypothesis that roughness merely changes surface stress but not the structure of the flow, at least in this channel flow and in agreement with the conclusions of Coceal *et al.* (2006).

Profiles of the long-time spatial averages of the mean velocity display log-law regions provided the area density of the cubical roughness (λ_p) exceeds about 10 %. The best log-law fits are provided when using a zero-plane displacement height (d') equal to the computed height at which the total surface drag force acts (Jackson 1981) and it has been demonstrated that this requires a value of von Kármán's coefficient κ significantly lower than the classical value of 0.41. Values of the log-law parameters are consistent with the implications of the results for smooth-wall flows of different classes (Nagib & Chauhan 2008), suggesting that there is no sudden jump in the nature of the near-wall flow as surface roughness increases from zero, which seems intuitively reasonable. It would be useful, however, to study fully rough cases with smaller roughness functions (and at high Reynolds number) to fill the gap between the smooth-wall data and the present very-rough-wall results. Only by jettisoning the definition of displacement height as the height at which the axial drag acts could (i) $\kappa = 0.41$ (or thereabouts) be maintained and (ii) κ remain fixed over all λ_p. But then, less satisfyingly, one would have to view d merely as a fitting coefficient, with no separately identifiable physical meaning, and then studies of such very rough surface flows could never be used to determine values of κ, whether in boundary layers or channels. Alternatively, if Jackson's assumptions are incorrect, some other physically-based definition of d might be correct and yield $\kappa = 0.41$, but none has thus far been proposed. Or, finally, one might argue that with such large roughness the expectation of a classical log law is in fact unreasonable.

The idea that κ is flow dependent might suggest that the whole foundation of the log law is fundamentally unsound, for it implies that (even at asymptotically high

https://doi.org/10.1017/S002211200999423X Published online by Cambridge University Press

Reynolds numbers) $u^+ \neq f(y^+)$ alone. Even if one believes that Reynolds number remained an influence in the various data assessed by Nagib & Chauhan (2008) and that, in the atmosphere, the measurement uncertainties are sufficiently great to preclude any reliable deductions about κ, the practical implications of flow-dependent κ would be significant, not least because it would lead to questions about the adequacy of commonly-accepted near-wall modelling approaches. This is partly why Spalart (P. Spalart, private communication, 2008) has suggested that any philosophy which admits that $u^+ = f(y^+ \textit{ and other things})$ is actually a 'frontal attack on the log law', not simply a refinement of it. The results shown in this paper, whilst not perhaps conclusive one way or the other, are nonetheless instructive.

We are grateful for support of visits by S. Leonardi to the Southampton group under their UK EPSRC Grant GR/S82947/01. Provision of substantial computer resources by the National Science Foundation through the TeraGrid resources provided by SDSC and TACC is also gratefully acknowledged, as are helpful discussions with the authors' colleagues, particularly Dr Gary Coleman.

REFERENCES

Andreas, E. L., Claffey, K. J., Jordan, R. E., Fairall, C. W., Guest, P. S., Persson, C. W. & Grachev, A. A. 2006 Evaluations of the von Kármán constant in the atmospheric surface layer. *J. Fluid Mech.* **559**, 117–149.

Andreas, E. L. & Trevino, G. 2000 Comments on 'A physical interpretation of von Kármán's constant based on asymptotic considerations – a new value'. *J. Atmos. Sci.* **57**, 1189–1192.

Bakken, O. M., Krogstad, P. A., Ashrafian, A. & Andersson, H. I. 2005 Reynolds number effects in the outer layer of the turbulent flow in a channel with rough walls. *Phys. Fluids* **17**, 065101.

Bhaganagar, K., Kim, J. & Coleman, G. 2004 Effect of roughness on wall-bounded turbulence. *Flow Turbul. Combust.* **72**, 463–492.

Breugrem, W. P., Boersma, B. J. & Uittenbogaard, R. E. 2006 The influence of wall permeability on turbulent channel flow. *J. Fluid Mech.* **562**, 35–72.

Castro, I. P. 2007 Rough-wall boundary layers: mean flow universality. *J. Fluid Mech.* **585**, 469–485.

Cheng, H. & Castro, I. P. 2002 Near wall flow over urban-like roughness. *Boundary-Layer Meteorol.* **104**, 229–259.

Cheng, H., Hayden, P., Robins, A. G. & Castro, I. P. 2007 Flow over cube arrays of different packing densities. *J. Wind Engng Ind. Aerodyn.* **95**, 715–740.

Coceal, O. & Belcher, S. E. 2004 A canopy model of mean winds through urban areas. *Q. J. R. Meteorol. Soc.* **130**, 1349–1372.

Coceal, O., Dobre, A., Thomas, T. G. & Belcher, S. E. 2007*b* Structure of turbulent flow over regular arrays of cubical roughness. *J. Fluid Mech.* **589**, 375–409.

Coceal, O., Thomas, T. G. & Belcher, S. E. 2007*a* Spatial variablity of flow statistics within regular building arrays. *Bound. Layer Meteorol.* **125**, 537–552.

Coceal, O., Thomas, T. G., Castro, I. P. & Belcher, S. E. 2006 Mean flow and turbulence statistics over groups of urban-like cubical obstacles. *Bound. Layer Meteorol.* **121**, 491–519.

Erm, L. P. & Joubert, P. N. 1991 Low-Reynolds-number turbulent boundary layers. *J. Fluid Mech.* **230**, 1–44.

Finnigan, J. 2000 Turbulence in plant canopies. *Annu. Rev. Fluid Mech.* **32**, 519–571.

Frenzen, P. & Vogel, C. A. 1995 On the magnitude and apparent range of variation of the von Kármán constant in the atmospheric surface layer. *Bound. Layer Meteorol.* **72**, 371–395.

Grimmond, C. S. B. & Oke, T. R. 1999 Aerodynamic properties of urban areas derived from analysis of surface form. *J. Appl. Meteorol.* **38**, 1262–1292.

Hagishima, A., Tanimoto, J., Nagayama, K. & Meno, S. 2009 Aerodynamics parameters of regular arrays of rectangular blocks with various geometries. *Bound. Layer Meteorol.* **132**, 315–338.

Ikeda, T. & Durbin, P. A. 2007 Direct simulations of a rough-wall channel flow. *J. Fluid Mech.* **571**, 235–263.

https://doi.org/10.1017/S002211200999423X Published online by Cambridge University Press

Jackson, P. S. 1981 On the displacement height in the logarithmic velocity profile. *J. Fluid Mech.* **111**, 15–25.

Kanda, M. 2006 Large-Eddy Simulations of the effects of surface geometry of building arrays on turbulent organized structures. *Bound. Layer Meteorol.* **118**. 151–168.

Kanda, M., Moriwaki, R. & Kasamatsu, F. 2004 Large-eddy simulation of turbulent organized structures within and above explicitly resolved cube arrays. *Bound. Layer Meteorol.* **112**, 343–368.

Kim, J. & Moin, P. 1985 Application of a fractional step method to incompressible Navier–Stokes equations. *J. Comput. Phys.* **59**, 308–223.

Krogstad, P.-A. & Antonia, R. A. 1999 Surface roughness effects in turbulent boundary layers. *Exp. Fluids* **27**, 450–460.

Leonardi, S., Orlandi, P., Smalley, R. J., Djenidi, L. & Antonia, R. A. 2003 Direct numerical simulations of turbulent channel flow with transverse square bars on one wall. *J. Fluid Mech.* **491**, 229–238.

Li, X., Zimmerman, N. & Princevac, M. 2008 Local imbalance of turbulent kinetic energy in the surface layer. *Bound. Layer Meteorol.* **129**, 115–136.

Macdonald, R. W. 2000 Modelling the mean velocity profile in an urban canopy layer. *Bound. Layer Meteorol.* **97**, 25–45.

Macdonald, R. W., Griffiths, R. F. & Hall, D. J. 1998 An improved method for the estimation of surface roughness of obstacle arrays. *Atmos. Environ.* **32**, 1857–1864.

Martilli, A. & Santiago, J. L. 2007 CFD simulations of airflow over a regular array of cubes. Part I. Three-dimensional simulation and validation with wind tunnel measurements. *Bound. Layer Meteorol.* **122**, 609–634.

Moser, R. D., Kim, J. & Mansour, N. N. 1999 Direct numerical simulation of turbulent channel flow up to $Re_\tau = 590$. *Phys. Fluids* **11**, 943–945.

Nagib, H. M. & Chauhan, K. A. 2008 Variations of von Kármán coefficient in canonical flows. *Phys. Fluids* **20**, 101518.

Oncley, S. P., Friehe, C., Larue, J. C., Businger, J. A., Itswheire, E. C. & Chang, S. S. 1996 Surface-layer fluxes, profiles and turbulence measurements over uniform terrain under near-neutral conditions. *J. Atmos. Sci.* **53**, 1029–1044.

Orlandi, P. 2000 *Fluid Flow Phenomena: A Numerical Toolkit*. Kluwer Academic.

Orlandi, P. & Leonardi, S. 2006 DNS of turbulent channel flows with two- and three-dimensional roughness. *J. Turbul.* **7**, 1–22.

Orlandi, P., Leonardi, S. & Antonia, R. A. 2006 Turbulent channel flow with either transverse or longitudinal roughness elements on one wall. *J. Fluid Mech.* **561**, 279–305.

Perry, A. E., Schofield, W. H. & Joubert, P. N. 1969 Rough wall turbulent boundary layers. *J. Fluid Mech.* **37**, 383–413.

Poggi, D., Porporato, A., Ridolfi, L., Albertson, J. D. & Katual, G. G. 2004 The effect of vegetation density on canopy sublayer turbulence. *Bound. Layer Meteorol.* **111**, 565–587.

Raupach, M. R., Finnigan, H. J. & Brunet, Y. 1996 Coherent eddies and turbulence in vegetation canopies: the mixing layer analogy. *Bound. Layer Meteorol.* **78**, 351–382.

Santiago, J. J., Coceal, O., Martilli, A. & Belcher, S. E. 2008 Variation of the sectional drag coefficient of a group of buildings with packing density. *Boundary-Layer Meteorol.* **128**, 445–457.

Stoesser, T., Mathey, F., Frohlich, J. & Rodi, W. 2003 LES of flow over multiple cubes. *Bulletin No.* 56. ERCOFTAC.

Vogel, C. A. & Frenzen, P. 2002 On reasons for the observed variation of the von Kármán constant in the atmospheric surface layer. In *Fifteenth Symposium on Boundary Layers and Turbulence*, American Meteorological Society, Wageningen, Holland, 15–19 July, pp. 422–423.

Xie, Z.-T. & Castro, I. P. 2006 LES and RANS for turbulent flow over arrays of wall-mounted cubes. *Flow Turbul. Combust.* **76** (3), 291–312.

Xie, Z.-T., Coceal, O. & Castro, I. P. 2008 Large-eddy simulation of flows over random urban-like obstacles. *Bound. Layer Meteorol.* **129**, 1–23.

https://doi.org/10.1017/S002211200999423X Published online by Cambridge University Press